ASME Letters in Dynamic Systems and Control
Online journal at:
https://asmedigitalcollection.asme.org/lettersdynsys

Motion Compensator for an Untethered Walking Insect Using Adaptive Model Predictive Control

Kaushik Rahman
Department of Mechanical Engineering,
Kennesaw State University,
Marietta, GA 30060
e-mail: krahman9@students.kennesaw.edu

Daniel Ehme
Department of Mechanical Engineering,
Kennesaw State University,
Marietta, GA 30060
e-mail: dehme@students.kennesaw.edu

Clint Penick
Ecology, Evolution & Organismal Biology,
Kennesaw State University,
Kennesaw, GA 30144
e-mail: cpenick1@kennesaw.edu

Dal Hyung Kim[1]
Department of Mechanical Engineering,
Kennesaw State University,
Marietta, GA 30060
e-mail: dkim97@kennesaw.edu

A locomotion compensator is normally utilized to observe the behavior of walking insects. These compensators cancel out the movement of freely walking insects to facilitate long-term imaging for studying behavior. However, controlling the locomotion compensator with a small error (≤ 1 mm) has been challenging due to the random motion of walking insects. This study introduces an adaptive model predictive control (MPC) approach combined with trajectory prediction to effectively control the transparent omnidirectional locomotion compensator (TOLC) for a randomly walking fire ant. The proposed MPC with prediction (MPCwP) utilizes the average velocity from the previous gaiting cycle to estimate its future trajectory. Experimental results demonstrate that MPCwP significantly outperforms MPC without prediction (MPCwoP), which relies solely on the current position and orientation. The distance error of the MPCwP method remains below 0.6 mm for 90.3% and 1.0 mm for 99.2% of the time, whereas MPCwoP achieves this only 32.6% and 69.1% of the time, respectively. Furthermore, the proposed method enhances the tracking performance of the heading angle, with the heading angle error staying below 8 deg for 92.6% of the time ($w_\theta = 1.0$). The enhanced performance of the proposed MPC has the potential to improve the observation images and enable the integration of additional equipment such as an optical microscope for brain or organ imaging. [DOI: 10.1115/1.4064370]

Keywords: adaptive control, biological systems applications, dynamics and control, model predictive control (MPC)

1 Introduction

The study of animal behavior can provide insight into diverse fields that include neuroscience, genetics, social evolution, biomechanics, and swarm intelligence. A major challenge for studies in animal behavior, however, has been the need for methods that precisely quantify behavior at scale. A potential solution has come in the form of automated tracking systems that can record and identify behaviors in real time [1,2]. However, tracking animal's behavior is a challenging problem because it requires keeping a target animal in the camera's field of view as it moves. This challenge is especially pronounced when observing small insects, such as ants and fruit flies, due to their random and fast movements.

To observe and track insect walking behavior, researchers often employed an automated robotic system that rotates the sphere in the desired direction to maintain the target insect's position within the field of view of the camera while it walks on the sphere [3–14]. Commercial setups like Ockenfels LC-100 [14] are inspired from the experimental setup of Kramer [5]. Recent versions of this device have introduced an omnidirectional locomotion compensator that simultaneously cancels the position and heading of the target animal [7,8,13]. While the tether-free locomotion compensator offers a promising method for observing small insects' behavior without motion restriction in infinite space, high-resolution imaging of their activities remains a challenging task due to the large positional errors due to their random movements. Conventional approaches have used proportional-integral-derivative (PID) control that compensates for errors without considering the random motion of the walking insect. Thus, the average error of these systems is typically a few millimeters, which represents a substantial error when compared to the size of a typical ant or fruit fly, which may be only 1–4 mm in total length.

This article presents an innovative adaptive model predictive control (MPC) method that enhances the tracking performance of the transparent omnidirectional locomotion compensator (TOLC) when observing a freely walking fire ant (*Solenopsis invicta*). The method employs a moving average algorithm to predict ant's movements and generate a target trajectory for control. The adaptive MPC approach is then employed to control the nonlinear model of the TOLC. The experimental results demonstrate that the proposed method enables highly precise and accurate high-resolution tracking and imaging of insect behavior, offering new possibilities for researchers studying animal behavior.

[1]Corresponding author.

Manuscript received July 12, 2023; final manuscript received November 28, 2023; published online January 29, 2024. Assoc. Editor: Biswanath Samanta.

2 Materials and Methods

2.1 TOLC System Overview. The TOLC is the active omnidirectional motion compensator for a walking insect using the transparent sphere [13]. Figures 1(*a*) and 1(*b*) show the overall schematic drawing and its implementation, respectively. While an insect is walking on top of the ball, the TOLC compensates insect's motion by rotating a transparent sphere using three omnidirectional wheels. The omnidirectional wheel is designed to achieve continuous contact with a sphere using alternated passive rollers, which creates a nearly continuous rotation of the sphere. The omnidirectional wheels were evenly placed at every 120 deg and oriented at 40 deg with respect to the *xy*-plane to support the sphere as shown in Figs. 1(*c*) and 1(*d*). Three DC servomotors are controlled to actuate omnidirectional wheels and the sphere. We utilized the optical sensor that measures the rotations of the sphere. Due to the noise of the optical sensor on the transparent sphere, the rotation of the sphere is determined by converting the measured motor rotations. We assumed that the slip between the omnidirectional wheels and sphere is negligible. The near-infrared (NIR) camera underneath the transparent sphere records the motion of the insect while NIR light-emitting diodes around the circumference of the sphere illuminate the insect motion from the bottom of the sphere. The dimensions and system parameters of the TOLC are described in Table 1.

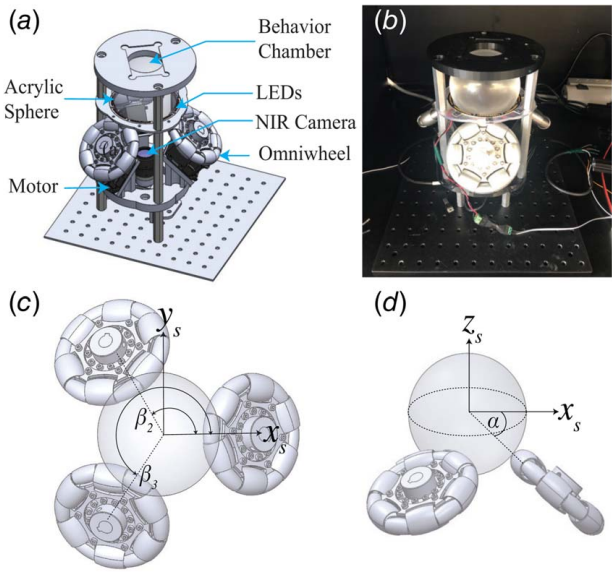

Fig. 1 Transparent omnidirectional locomotion compensator: (*a*) overall schematic drawings, (*b*) experimental setup, (*c*) top view, and (*d*) side view

Table 1 Dimensions and system parameters

Description (symbol)	Value (unit)
Radius of sphere (r_{sp})	50.8 mm
Radius of omnidirectional wheel (r_w)	50.0 mm
Tilt angle (from *xy*-plane) (α)	40 deg
Distribution angle of wheel (β)	[0 deg, 120 deg, 240 deg]
Unit torque of motor (k_t)	0.4 N · m
Mass of sphere (m)	0.648 kg
Damping coefficient (b)	0.025 N · m · s/rad
Input delay (t_d)	0.04 s
Moment of inertia (sphere) (I)	6.89×10^{-4} kg · m^2
Sampling time (dt)	5 ms

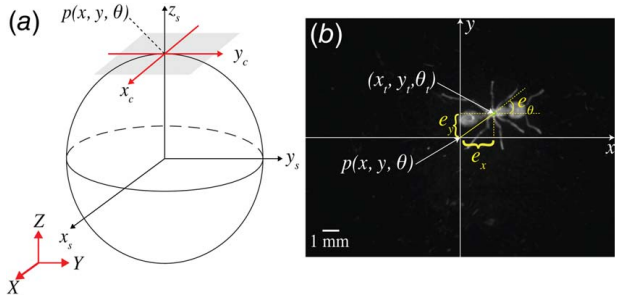

Fig. 2 TOLC dynamic model. (*a*) Schematic drawing. Gray plane: Image plane where an ant is walking. (*b*) The NIR image of a walking ant. The sphere position (x, y, θ) is the center of the image. The error is defined as (e_x, e_y, e_θ), and the ant position is (x_t, y_t, θ_t).

2.2 System Model. The sphere of the TOLC rotates without translation since it is on top of three omnidirectional wheels. Throughout the control process, a walking insect is positioned on the upper surface of the sphere, and the image frame (x, y, θ) in Fig. 2 represents the position of the TOLC. A posture of an insect (x_t, y_t, θ_t) in Fig. 2(*b*) is defined as follows:

$$[x_t, y_t, \theta_t]^T = [x, y, \theta]^T + [e_x, e_y, e_\theta]^T \tag{1}$$

where the error on the image plane is $[e_x, e_y, e_\theta]^T$. The image coordinate frame can rotate in z-axis only, not in x- and y-axis, so that the image plane is always at the top of the sphere while rotating when an insect turns. We formulated the following TOLC model as follows (see Supplemental Materials on the ASME Digital Collection):

$$\begin{cases} \dot{x} = r_{sp}\{\dot{\theta}_x \sin(\theta_z) + \dot{\theta}_y \cos(\theta_z)\} \\ \dot{y} = r_{sp}\{\dot{\theta}_x \cos(\theta_z) - \dot{\theta}_y \sin(\theta_z)\} \\ \dot{\theta} = \dot{\theta}_z \\ \ddot{\theta}_x = -\dfrac{b}{I}\dot{\theta}_x + \left(\dfrac{k_t r_w}{I r_{sp}}\right) s\alpha\left(c\beta_1 u_1 + c\beta_2 u_2 + c\beta_3 u_3\right) \\ \ddot{\theta}_y = -\dfrac{b}{I}\dot{\theta}_y + \left(\dfrac{k_t r_w}{I r_{sp}}\right) s\alpha\left(s\beta_1 u_1 + s\beta_2 u_2 + s\beta_3 u_3\right) \\ \ddot{\theta}_z = -\dfrac{b}{I}\dot{\theta}_z + \left(\dfrac{k_t r_w}{I r_{sp}}\right) \dfrac{c\alpha}{3}(u_1 + u_2 + u_3) \end{cases} \tag{2}$$

where θ_x, θ_y, and θ_z represent the angular position of the sphere in the x-, y-, and z-axis, respectively. u_i is a control input for the ith motor, and s and c are trigonometric functions sine and cosine.

2.3 Adaptive Model Predictive Control. The dynamic model of the TOLC shown in Eq. (2) is a nonlinear model due to the sinusoidal functions. Thus, the adaptive model predictive control is implemented for the TOLC by linearization, which updates the model parameters in real time. Equation (2) can be rewritten in a matrix form as follows:

$$\begin{aligned} \dot{X} &= AX + BU \\ Y &= CX \end{aligned} \tag{3}$$

where a state vector $X = [x, y, \theta, \dot{\theta}_x, \dot{\theta}_y, \dot{\theta}_z]^T$, an input vector U = $[u_1, u_2, u_3]^T$, and the state-space matrices A, B, and, C are given

as follows:

$$A = \begin{bmatrix} & r_{sp}\sin\theta_z & r_{sp}\cos\theta_z & 0 \\ & -r_{sp}\cos\theta_z & r_{sp}\sin\theta_z & 0 \\ & 0 & 0 & 1 \\ 0_{6\times3} & -b/I & 0 & 0 \\ & 0 & -b/I & 0 \\ & 0 & 0 & -b/I \end{bmatrix}$$
$$B = \frac{k_t r_w}{I r_{sp}} \begin{bmatrix} & 0_{3\times3} & \\ s\alpha c\beta_1 & s\alpha c\beta_2 & s\alpha c\beta_3 \\ s\alpha s\beta_1 & s\alpha s\beta_2 & s\alpha s\beta_3 \\ \frac{c\alpha}{3} & \frac{c\alpha}{3} & \frac{c\alpha}{3} \end{bmatrix} \quad (4)$$
$$C = \begin{bmatrix} I_{3\times3} & 0_{3\times3} \end{bmatrix}$$

To linearize the matrix A, we assumed that the change of θ_z is negligible in short duration so that θ_z is approximated as $\theta_{z,k}$, a rotation angle at the current step k. Then, $\sin\theta_z$ and $\cos\theta_z$ are replaced as a constant value as $\sin\theta_{z,k}$ and $\cos\theta_{z,k}$. The matrix A is updated in every step for linearization. Then, the linear time invariant (LTI) and discrete model for adaptive model predictive control is expressed as follows:

$$X_{k+1} = \overbrace{(Adt + I)}^{\widetilde{A}} X_k + \overbrace{Bdt}^{\widetilde{B}} U_k, \quad k = 0, 1, 2, \ldots n \quad (5)$$
$$Y_k = CX_k$$

The predictive state at each future step is expressed from the discrete model in Eq. (5) as follows:

$$Y_{\rightarrow k+1} = PX_k + SU_{\rightarrow k-N_d} + HU_{\rightarrow k} \quad (6)$$

where $Y_{\rightarrow k+1}$ is the future output states after step k, X_k is the current state of the system, $U_{\rightarrow k-N_d}$ is the committed inputs during the delay in the past, and $U_{\rightarrow k}$ is the future inputs. The matrices P, S, and H are obtained from the state-space matrices as follows:

$$X_{\rightarrow k+1} = \begin{bmatrix} X_{k+1\,|\,k} & \ldots & X_{k+N_p\,|\,k} \end{bmatrix}^T$$
$$Y_{\rightarrow k+1} = \begin{bmatrix} Y_{k+1\,|\,k} & \ldots & Y_{k+N_p\,|\,k} \end{bmatrix}^T$$
$$U_{\rightarrow k-N_d} = \begin{bmatrix} U_{k-N_d} & \ldots & U_{k-1} \end{bmatrix}^T$$
$$U_{\rightarrow k} = \begin{bmatrix} U_{k\,|\,k} & \ldots & U_{k+N_C-1\,|\,k} \end{bmatrix}^T$$
$$P = \begin{bmatrix} C\widetilde{A} & C\widetilde{A}^2 & \ldots & C\widetilde{A}^{N_p} \end{bmatrix}^T \quad (7)$$
$$S_{ij} = \begin{cases} 0 & (i < j) \\ C\widetilde{A}^{i-j}\widetilde{B} & (1 \le i \le N_p,\ 1 \le j \le N_d) \end{cases}$$
$$H_{ij} = \begin{cases} 0 & (1 \le i \le N_c \text{ or } i < j) \\ C\widetilde{A}^{i+j-N_c-N_d}\widetilde{B} & (N_c < i \le N_p,\ 1 \le j \le N_c) \end{cases}$$

where N_p is a prediction horizon, N_c is a control horizon, and N_d represents steps of delay. We set $N_p = 12$, $N_c = 4$, and $N_d = 8$ from the measurement of the system.

The purpose of MPC is to minimize the error between the predicted output and the reference input trajectory. Therefore, the cost function can be contracted as follows:

$$J = W\|Y_{\rightarrow k+1} - \hat{Y}_{\rightarrow k+1}\|^2 + \lambda\|u_{\rightarrow i+1}\|^2 \quad (8)$$

where $\hat{Y}_{\rightarrow k+1}$ is a reference input trajectory, W is the weight matrix, and λ is a regularization gain. The role of λ is to penalize a higher input to avoid an unnecessary aggressive input. The weight matrix W is set as follows to weigh the priority of tracking between the position error and orientation error:

$$W = \mathrm{diag}\left(\begin{bmatrix} 1 & 1 & w_\theta & \ldots & 1 & 1 & w_\theta \end{bmatrix}\right) \quad (9)$$

where diag $(\cdot)$ represents a diagonal matrix with the specified elements on the diagonal and w_θ is a weight factor of heading. If w_θ is set as 0, the position error is only compensated while the orientation error is ignored. Since the proposed system becomes the LTI system after linearization, the least square method is implemented to find the optimal solution of Eq. (9).

2.4 Prediction of Ant Trajectory. The cost function in Eq. (9) is minimized when the difference between the predicted output trajectory $Y_{\rightarrow k+1}$ and the reference input $\hat{Y}_{\rightarrow k+1}$ is minimized. Since $\hat{Y}_{\rightarrow k+1}$ is a future trajectory of random walking of an insect, the prediction of an insect's motion is critical for the proposed MPC method. The MPC with prediction (MPCwP) is achieved by setting a future walking trajectory of the insect as an input reference trajectory. The MPC without prediction (MPCwoP) sets the input reference trajectory as a current position and orientation only. To obtain a future trajectory of a walking insect, we implemented a simple prediction method, a moving average. First, an average vector $(\bar{x}_{t,k}, \bar{y}_{t,k})$ of the movement at the current step k is computed from the position of the insect in the previous n_{mov} steps as follows:

$$(\Delta\bar{x}_{t,k}, \Delta\bar{y}_{t,k}) = \frac{\sum_{i=1}^{n_{\mathrm{mov}}} \left(x_{t,k-i+1} - x_{t,k-i},\ y_{t,k-i+1} - y_{t,k-i}\right)}{n_{\mathrm{mov}}} \quad (10)$$

Then, the next positions in the future ith step are projected by concatenating the average vector $(\bar{x}_{t,k}, \bar{y}_{t,k})$ from the current insect position $(x_{t,k}, y_{t,k})$:

$$x_{t,k+1} = x_{t,k} + i \cdot \Delta\bar{x}_{t,k}$$
$$y_{t,k+1} = y_{t,k} + i \cdot \Delta\bar{y}_{t,k} \quad (11)$$

The average gaiting cycle of the walking ant is around 120 ms (~8 Hz gait cycle). Thus, the window for moving average is 12 steps, which is the same as half of the average gaiting cycle of the ant. Thus, the proposed method estimates the future trajectory of the walking insect from an average velocity vector of the previous gaiting cycle. When the ant walks continuously at the same speed, the controller compensates the error effectively using the predicted trajectory of the walking ant. However, when an ant changes its speed or direction, the error increases due to the limitation of the prediction method. Figure 3 shows the overall control flow of the proposed MPC method for the TOLC.

2.5 Fire Ant Husbandry. We collected queenright colonies of the red imported fire ant (*Solenopsis invicta*) from the area surrounding Kennesaw State University (Marietta, GA). We separated workers and brood from the soil using the water drip method [15], and colonies were then housed in plastic containers with a water tube plugged with a cotton ball to serve as a nesting chamber. Colonies were maintained on a 12:12 light/dark cycle at 25 °C and received 20% sucrose solution, dead beetle larvae (*Zophobas morio*), and Bhatkar diet ad libitum [16]. Before experiments, we placed the ant on the apparatus for 5 min to acclimate prior to data collection. After each experiment, we provided 30 min of "cool" time for the ants to get its strength back. The experiment was conducted in a dark environment at room temperature.

3 Results and Discussion

The results in Fig. 4 demonstrate the walking motion achieved with MPCwP. Figure 4(*a*) shows the sequence of images and the path taken by the ant and TOLC while walking with a small turn. The ant was at the origin at $t = 0$ s, and the path undergoes fluctuations as the ant turns, eventually moving straight after 0.55 s, as shown in Figs. 4(*a*)–4(*e*). Figure 4(*f*) shows a significant distance error of over 1 mm after its initial turn (~0.2 s) and completion of turning (0.55 s) because the predicted trajectory deviated from the actual movement. During straight motion after 0.55 s, the average distance error (e_d) reduces to 0.393 mm because the prediction agrees well with the actual movement. In Fig. 4(*g*), the heading error experiences an initial increase from 0 to 20 deg while

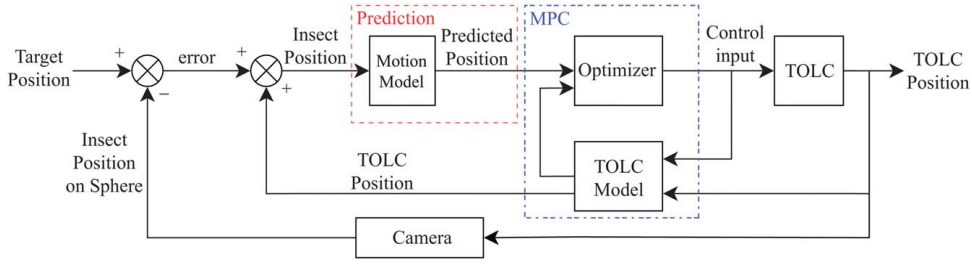

Fig. 3 Control flow of the MPC method for TOLC

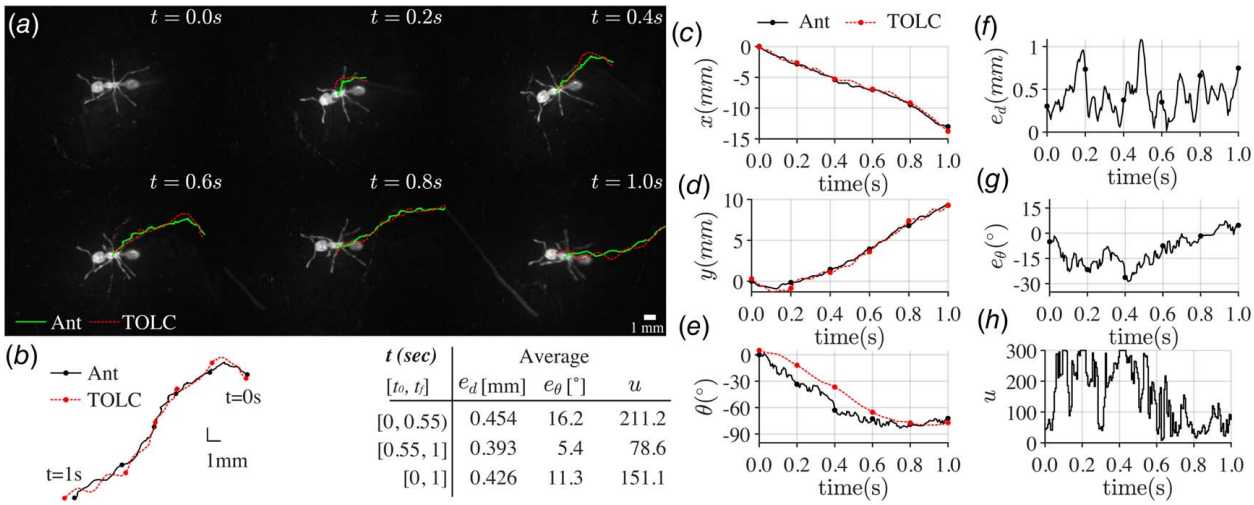

Fig. 4 Omnidirectional control with MPCwP ($w_\theta = 0.4$) with $n_{mov} = 12$ steps, $\lambda = 0.015$ (See Supplement Video 1 available in the Supplemental Materials on the ASME Digital Collection). (*a*) Image sequences for 1 s. (*b*) Trajectories. Position in (*c*) *x*-axis and (*d*) *y*-axis. (*e*) Heading. (*f*) Distance error. (*g*) Heading error. (*h*) Sum of control inputs (three motors). The table shows the average values for (*f*)–(*h*) before and after turning (0.55 s). (See Supplemental Figure 1 available in the Supplemental Materials on the ASME Digital Collection for comparable result of MPCwoP.)

turning and further increases to 30 deg at around 0.4 s. In Fig. 4(*h*), the average inputs before and after turning (at 0.55 s) stand at 211.2 and 78.6, respectively, indicating that a larger input is required to effectively compensate for the heading angle error.

The simulated outcomes presented in Fig. 5 provide a comparative analysis between MPCwP, MPCwoP, and PID when $w_\theta = 0.0$. In this simulation, the actual movements of the ant in Fig. 4 are utilized as input. As shown in Figs. 5(*a*) and 5(*b*), the trajectory of MPCwoP and PID lag behind the ant, while the trajectory of MPCwP closely tracks ant's movements. Consequently, the distance error (e_d) of MPCwoP and PID exceed 1 mm for most of the duration, as shown in Fig. 5(*c*), which is notably higher than that of MPCwP. The average values of e_d for MPCwP, MPCwoP, and PID were 0.390 mm, 1.17 mm, and 1.19 mm, respectively. However, MPCwP requires higher inputs to effectively compensate for the error. As shown in Fig. 5(*d*), the control inputs remain relatively low for MPCwoP (averaging at 19.4) and PID (averaging at 25.4) compared to MPCwP (averaging at 31.9).

The findings presented in Fig. 6 provide a performance comparison of MPCwP under varying values of the parameter w_θ. It is observed that the heading error in Fig. 6(*b*) tends to be improved with higher values of w_θ due to more aggressive compensation. However, this improvement in heading error comes at the cost of an increased distance error, as shown in Fig. 6(*a*), indicating a trade-off between heading and distance error, which can be utilized for behavior observation with the directional stimuli. Furthermore, Fig. 6(*c*) reveals that larger control inputs are required to enhance the heading error with higher values of w_θ. This implies that as w_θ increases, a more substantial control effort is necessary to effectively address the heading error.

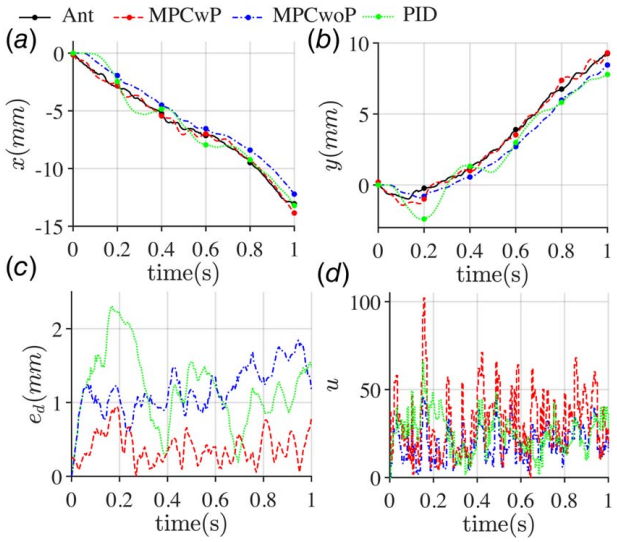

Fig. 5 Performance comparison between MPCwP, MPCwoP, and PID (position control with $w_\theta = 0.0$, $n_{mov} = 12$ steps, and $\lambda = 0.015$). Position in (*a*) *x*-axis and (*b*) *y*-axis. (*c*) Distance error. (*d*) Sum of control inputs (three motors).

Since an ant walks randomly, the performance of the TOLC is determined by the accuracy of the predicted future positions of a walking ant. As illustrated in Figs. 7(*a*) and 7(*b*), the distribution

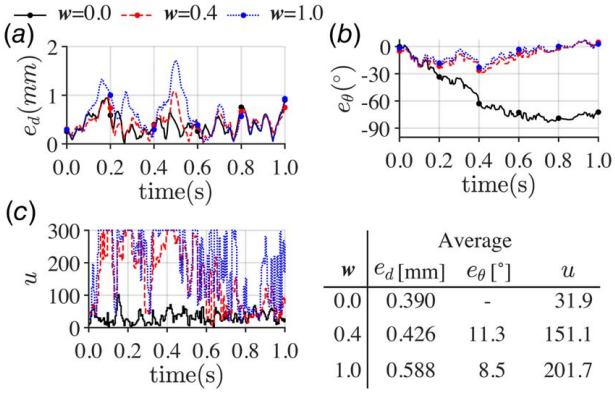

	Average		
w	e_d [mm]	e_θ [°]	u
0.0	0.390	-	31.9
0.4	0.426	11.3	151.1
1.0	0.588	8.5	201.7

Fig. 6 Performance comparison of the TOLC for w_θ = 0.0, 0.4, 1.0 (n_{mov} = 12 steps and λ = 0.015). (*a*) Distance error. (*b*) Heading error. (c) Sum of control inputs (three motors). The table shows average values of the result presented in (*a*)–(c).

of ant positions for MPCwoP is wider and extends beyond the target position at the origin, whereas for MPCwP, it is more concentrated around the target position. The average position of MPCwoP along the longitudinal axis is 0.796 mm, which increases with faster walking speed. Figure 7(*b*) shows the distribution of position error in longitudinal axis at different speed. The frequency is normalized between 0 and maximum value. Each graph from top to bottom shows the following data: 0–10, 10–20, 20–30, and above 30 mm/s. The average position in the longitudinal axis for a walking speed is under 10, 10–20, 20–30, and over 30 mm/s, whose average is 0.555, 0.900, 1.10, and 1.17 mm respectively. On the other hand, the average position for MPCwP is located at 0.23 mm, which is 71.3% less than that of MPCwoP. Even though the walking speed increases, the position error in the longitudinal axis only increases slightly (Fig. 7(*b*)) as 0.286, 0.348, 0.380, and 0.417 mm for a walking speed under 10, 10–20, 20–30, and over 30 mm/s respectively. In terms of e_d, Fig. 7(*c*) shows that MPCwP outperforms MPCwoP, keeping e_d below 0.6 mm for 90.3% of the time, while MPCwoP kept it for 32.6%. Additionally, the MPCwP keeps e_d under 1 mm for 99.2% of the time, while MPCwoP only achieves this for 69.1%. Figure 7(*d*) presents the overall distribution of distance error against gaiting speed, showing that MPCwP maintains a low position error (under 0.5 mm) even at higher walking speeds, while the error of MPCwoP continues to increase. This comparison clearly indicates that prediction is a critical factor in the MPC for the TOLC.

The TOLC exhibits better heading angle tracking performance with higher values of w_θ. Figure 8 illustrates the performance of the TOLC for two different values of the control parameter, w_θ = 0.4 and 1.0. Figure 8(*a*) shows the distribution of ants' positions for w_θ = 0.4 (left) and 1.0 (right), indicating that the distribution of positions for w_θ = 0.4 is slightly smaller than that for w_θ = 1.0. In Fig. 8(*b*), it is shown that the heading angle error is less than 8 deg for 83.8% of the time for w_θ = 0.4 (red) and 92.6% for w_θ = 1.0 (gray). It is observed that the aggressive control of heading error decreases the performance of position tracking despite using larger inputs for control. The average distance errors for w_θ = 0.4 and 1.0 are 0.312 and 0.355 mm, respectively.

To assess the effectiveness of TOLC performance, we conducted simulations using experimentally measured ant movements as identical inputs for each method. The results in Fig. 9 show that MPCwP

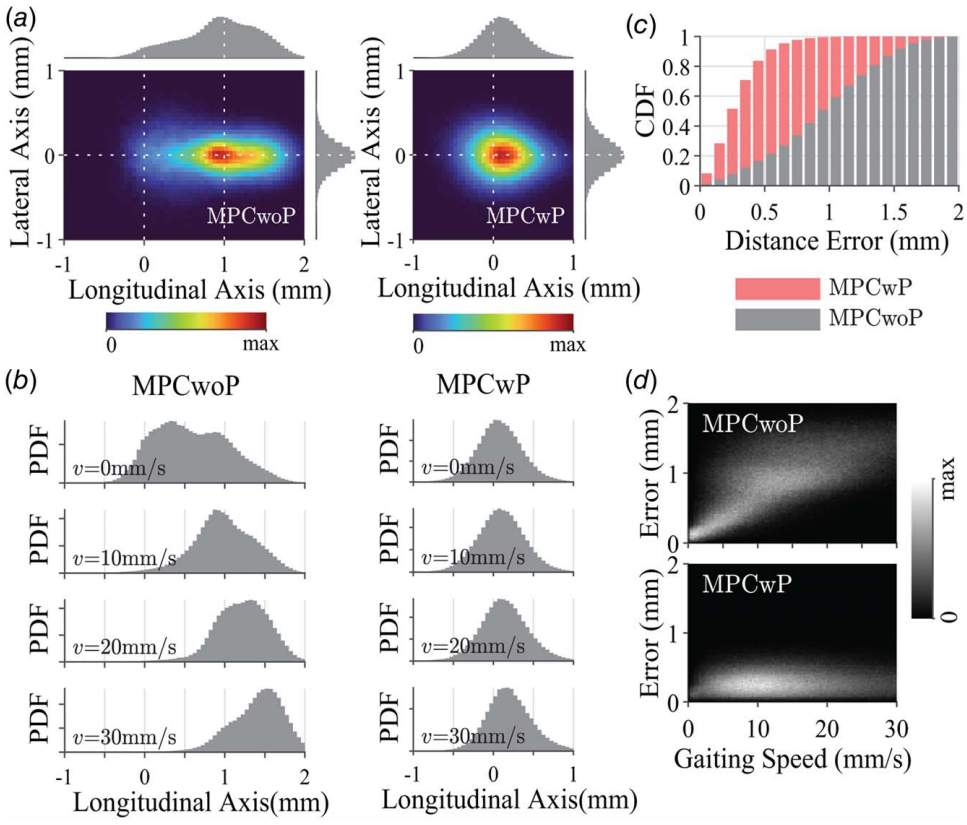

Fig. 7 Comparison between MPCwP and MPCwoP methods. The data were collected from 17 ants (8 for MPCwP and 9 for MPCwoP) for 81.3 and 95.2 min, respectively. (*a*) Distribution of position error. The distribution in the longitudinal (top), lateral direction (right), and two-dimensional space (center). (*b*) Distribution of position error at different speeds. (c) Cumulative distribution of the distance error. (*d*) Distance error distribution at different gaiting speeds.

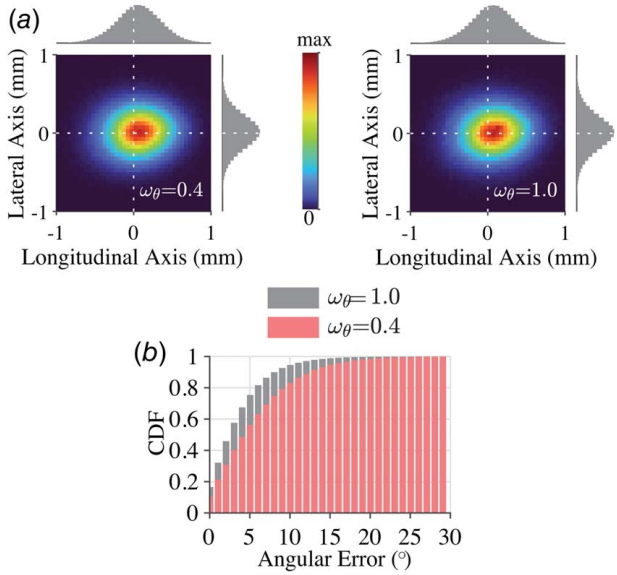

Fig. 8 Performance of the TOLC for $w_\theta = 0.4$ and 1.0. Data were collected for $\lambda = 0.015$ and $n_{mov} = 12$ from five ants for 50.1 and 52.9 min, respectively. (*a*) Two-dimensional distribution of positions for a walking insect. (*b*) Cumulative distribution of the heading angle error.

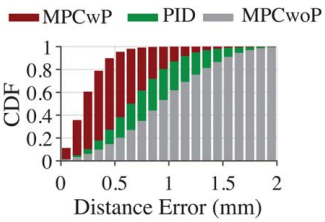

Fig. 9 Simulated performance comparison between MPCwP, PID, and MPCwoP. All data were collected from 10 different ants for 315.0 minutes. Cumulative distribution of the distance error.

outperforms both MPCwoP and PID, keeping e_d below 0.6 mm for 95.4% of the time, while PID and MPCwoP kept it for 38.2% and 20.2% of the time, respectively. Additionally, the MPCwP keeps e_d under 1 mm for 99.8% of the time, while PID and MPCwoP only achieves this for 80.4% and 53.2%, respectively.

4 Conclusion

In this article, we have demonstrated the adaptive MPC to control the TOLC with the prediction of a future trajectory of a walking fire ant. The MPC controller optimizes control inputs to minimize position and heading errors between the TOLC and the anticipated trajectory of the ant. A moving average scheme is employed to predict ant's future trajectory, and the state-space matrix parameters are updated in real time. The proposed MPCwP successfully keeps the ant within a distance error of 0.6 mm for 90.3% of the time, compared to 32.6% during MPCwoP. Increasing the weighting factor for heading angle introduces a trade-off between position tracking and heading error. The MPCwP maintains low position errors even at higher walking speeds, in contrast to increased errors in MPCwoP. Experimental evaluations and parameter variations validate the effectiveness of the proposed MPC, providing valuable insights for future research on insect mobility, biomechanics, and sensory responses without constraining their movement. The improved performance of the proposed MPC could enhance observation image quality and enable the integration of additional equipment, like an optical microscope for brain or organ imaging.

Conflict of Interest

There are no conflicts of interest.

Data Availability Statement

The datasets generated and supporting the findings of this article are obtainable from the corresponding author upon reasonable request.

References

[1] Guo, X., Lin, M. R., Azizi, A., Saldyt, L. P., Kang, Y., Pavlic, T. P., and Fewell, J. H., 2022, "Decoding Alarm Signal Propagation of Seed-Harvester Ants Using Automated Movement Tracking and Supervised Machine Learning," Proc. R. Soc. B, **289**(1967), p. 20212176.
[2] Veeraraghavan, A., Chellappa, R., and Srinivasan, M., 2008, "Shape-and-Behavior Encoded Tracking of Bee Dances," IEEE. Trans. Pattern. Anal. Mach. Intell., **30**(3), pp. 463–476.
[3] Götz, K. G., and Wenking, H., 1973, "Visual Control of Locomotion in the Walking Fruitfly Drosophila," J. Comp. Physiol., **85**, pp. 235–266.
[4] Arnold, S. E., Stevenson, P. C., and Belmain, S. R., 2016, "Shades of Yellow: Interactive Effects of Visual and Odour Cues in a Pest Beetle," PeerJ, **4**, p. e2219.
[5] Kramer, E., 1976, "The Orientation of Walking Honeybees in Odour Fields With Small Concentration Gradients," Physiol. Entomol., **1**(1), pp. 27–37.
[6] Weber, T., Thorson, J., and Huber, F., 1981, "Auditory Behavior of the Cricket," J. Comp. Physiol., **141**, pp. 215–232.
[7] Iwatani, Y., Ogawa, H., Shidara, H., Sakura, M., Sato, T., Hojo, M. K., Honma, A., and Tsurui-Sato, K., 2019, "Markerless Visual Servo Control of a Servosphere for Behavior Observation of a Variety of Wandering Animals," Adv. Robot., **33**(3–4), pp. 183–194.
[8] Iwatani, Y., 2021, "High-Speed Servosphere," IEEE/SICE International Symposium on System Integration (SII), Iwaki, Fukushima, Japan, Jan. 11–14, IEEE, pp. 613–618.
[9] Shigaki, S., Fukushima, S., Kurabayashi, D., Sakurai, T., and Kanzaki, R., 2016, "A Novel Method for Full Locomotion Compensation of an Untethered Walking Insect," Bioinspir. Biomim., **12**(1), p. 016005.
[10] Otálora-Luna, F., Dickens, J. C., Brinkerhoff, J., and Li, A. Y., 2022, "Behavior of Nymphs and Adults of the Black-Legged Tick Ixodes Scapularis and the Lone Star Tick Ambylomma Americanum in Response to Thermal Stimuli," Insects, **13**(2), p. 130.
[11] Nagaya, N., Mizumoto, N., Abe, M. S., Dobata, S., Sato, R., and Fujisawa, R., 2017, "Anomalous Diffusion on the Servosphere: A Potential Tool for Detecting Inherent Organismal Movement Patterns," PLoS. One., **12**(6), p. e0177480.
[12] Goulard, R., Buehlmann, C., Niven, J. E., Graham, P., and Webb, B., 2020, "A Motion Compensation Treadmill for Untethered Wood Ants (Formica rufa): Evidence for Transfer of Orientation Memories From Free-Walking Training," J. Exp. Biol., **223**(24), p. jeb228601.
[13] Pun, P., Brown, J., Cobb, T., Wessells, R. J., and Kim, D. H., 2021, "Navigation of a Freely Walking Fruit Fly in Infinite Space Using a Transparent Omnidirectional Locomotion Compensator (TOLC)," Sensors, **21**(5), p. 1651.
[14] van Tilborg, M., van der Pers, J. N., Roessingh, P., and Sabelis, M. W., 2003, "State-Dependent and Odor-Mediated Anemotactic Responses of a Micro-Arthropod on a Novel Type of Locomotion Compensator," Beh. Res. Meth., Instr. Comp., **35**, pp. 478–482.
[15] Banks, W. A., Lofgren, C., Jouvenaz, D., Stringer, C., Bishop, P., Williams, D., Wojcik, D., and Glancey, B., 1981, "Techniques for Collecting, Rearing, and Handling Imported Fire Ants," U.S. Dep. Agric. Sci. Educ. Adm, **21**, pp. 1–9.
[16] Bhatkar, A., and Whitcomb, W., 1970, "Artificial Diet for Rearing Various Species of Ants," Florida Entomol., **53**(4), pp. 229–232.